Electronic Supplementary Material (ESI) for RSC Advances.

Supporting information

For

Effects of Ti-doping amount and annealing temperature on electrochromic performance of sol-gel derived WO_3

Hee sung Park[ab], Sunghyeok Park[ac], Seung Han Song[ab], Dao Thi Thuy[ac], Hung Van Tran[ac], Seok In Lee[ad], Churl Hee Cho[*b], Chi-Hwan Han[*a] and Sungjun Hong[*a]

[a] *Photovoltaic Laboratory, New and Renewable Energy Research, Korea Institute of Energy Research, 152 Gajeong-ro , Yuseong-gu, Daejeon 34125, Republic of Korea.*

[b] *Department of Energy Science and Technology, Chungnam National University, 99 Daehak-ro, Yuseong-gu, Daejeon 35015, Republic of Korea*

[c] *Renewable Energy Engineering, University of Science and Technology, 217, Gajeoung-ro, Yuseong-gu, Daejeon 34113, Republic of Korea.*

[d] *Department of Chemistry, Korea University, Seoul 02741, Republic of Korea*

[*]Corresponding author (C-H Cho., C.-H. Han., S-J Hong.)

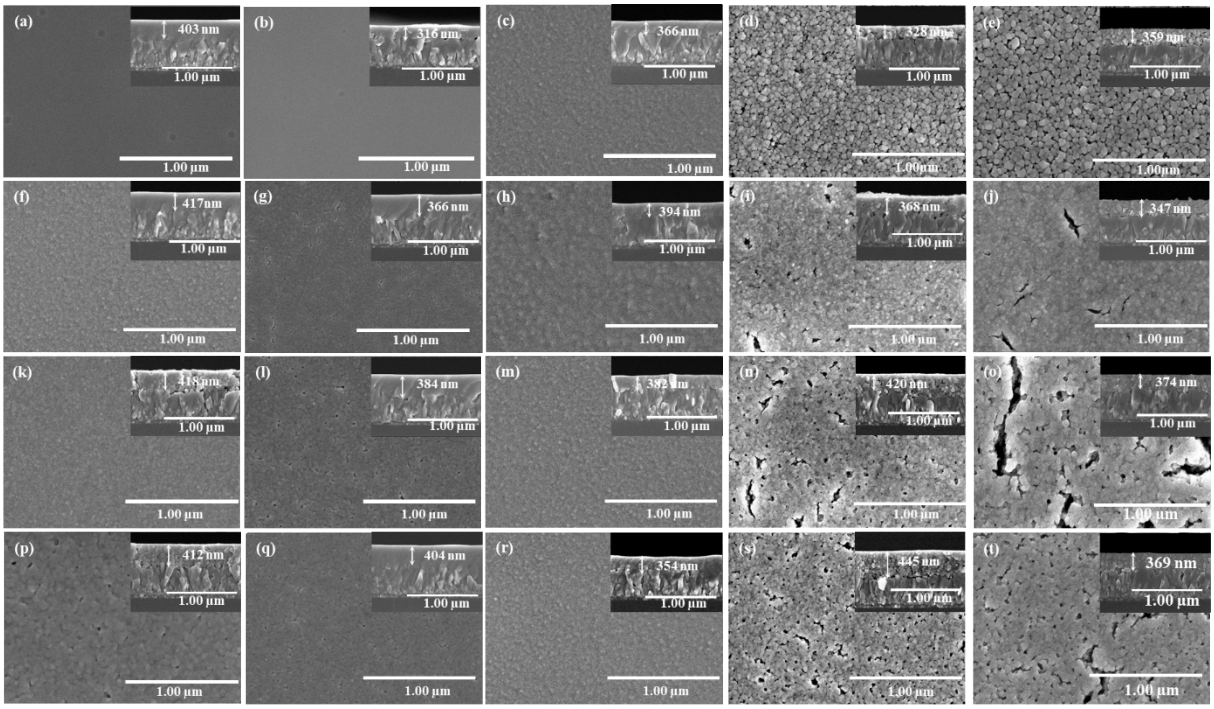

Figure S1. SEM surface and cross-sectional images of (1st row) 4Ti-WO_3, (2nd row) 12Ti-WO_3, (3rd row) 16Ti- WO_3 and (4th row) 20Ti- WO_3 films annealed at 200, 250, 300, 350 and 400 °C from left to right, respectively.

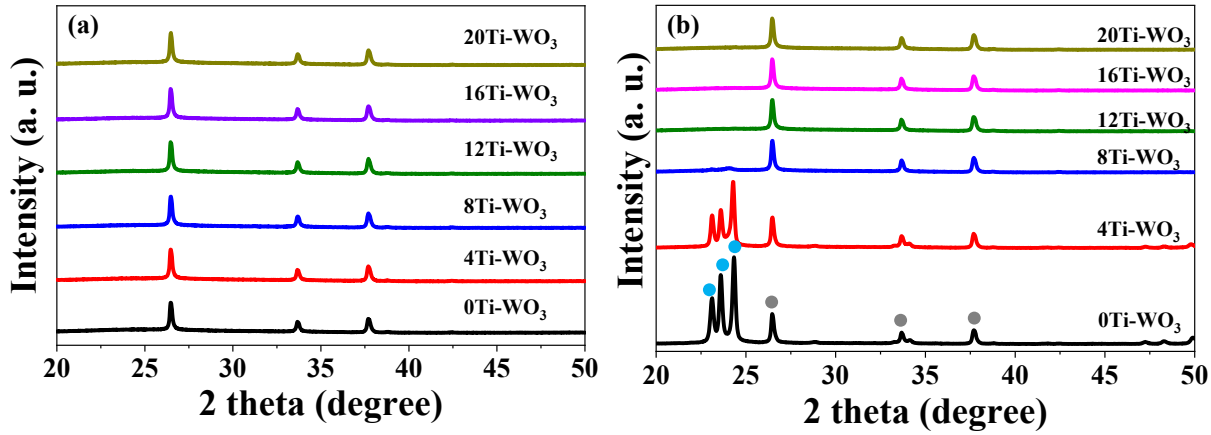

Figure S2. XRD patterns of neat and respective TCA doped WO_3 films annealed at (a) 250 and (b) 350 °C. (The light blue and grey circles refer to monoclinic WO_3 and FTO substrate, respectively.)

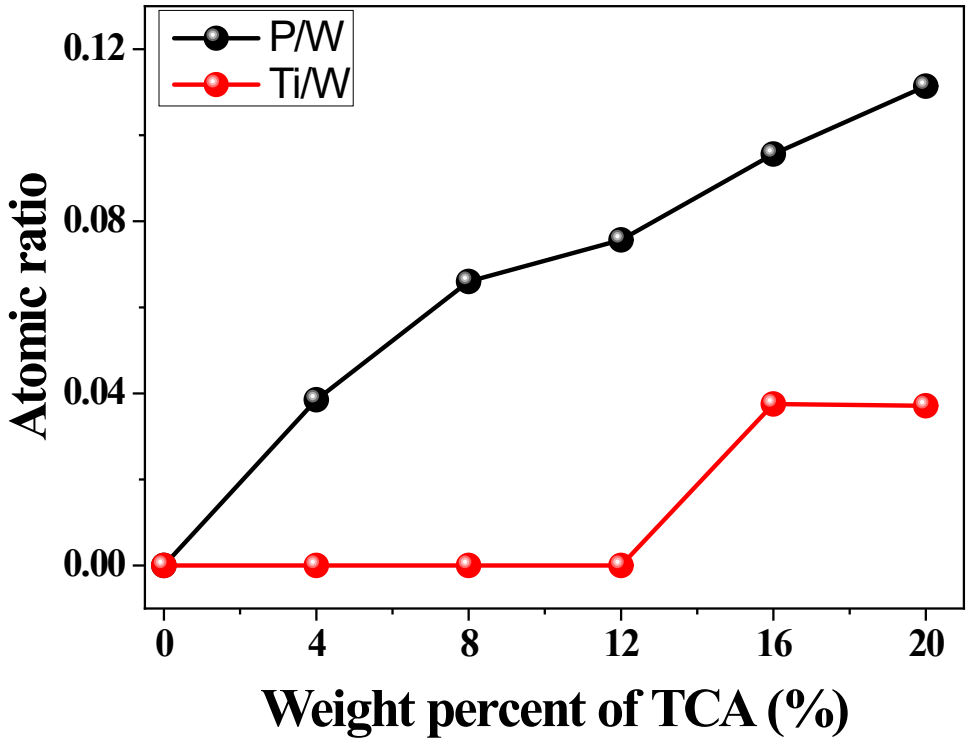

Figure S3. Atomic ratios of P/W or Ti/W for xTi-WO_3-300 samples determined with EDS.

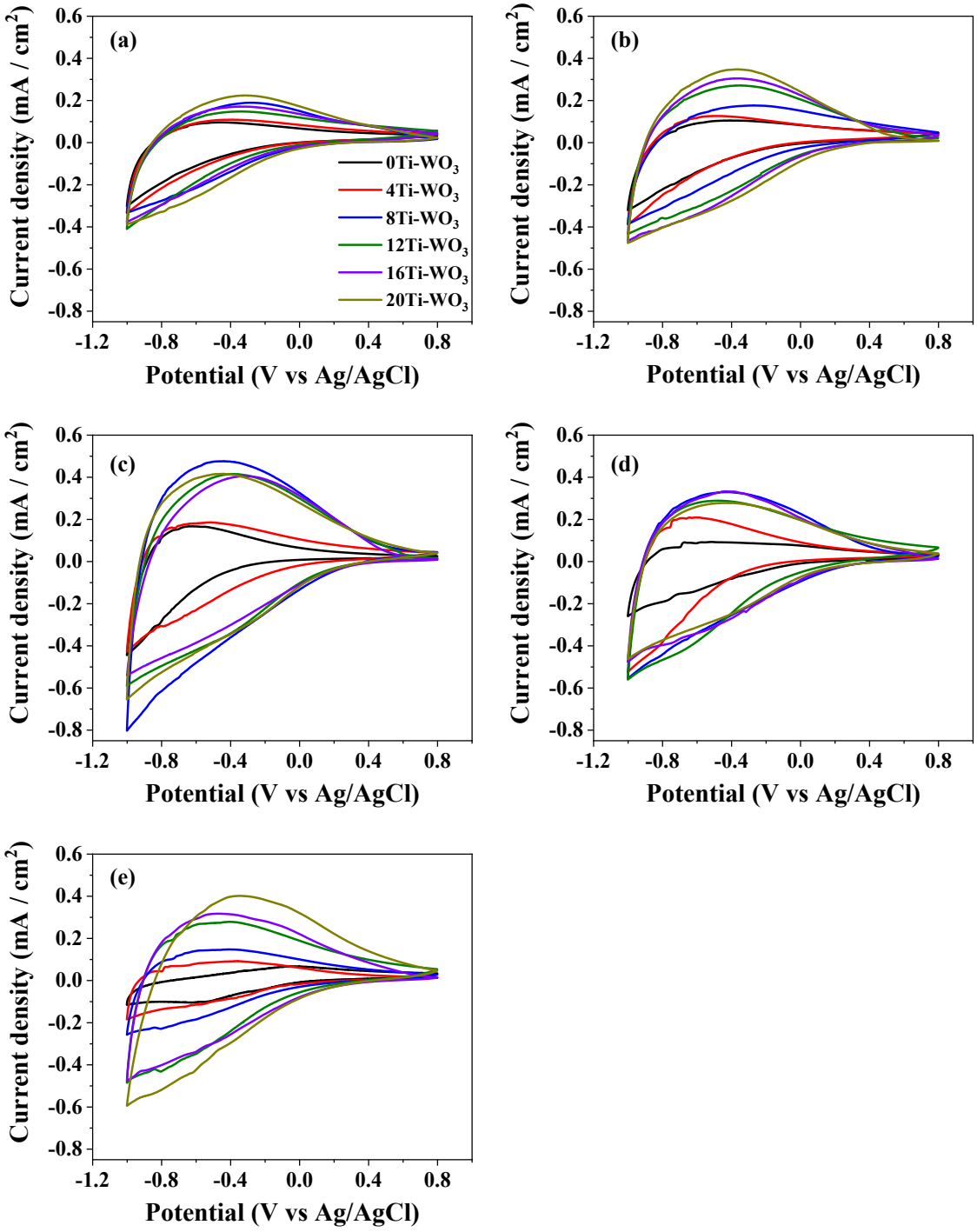

Figure S4. Cyclic voltammograms of various WO_3 films annealed at (a) 200, (b) 250, (c) 300, (d) 350, and (e) 400 °C, respectively.

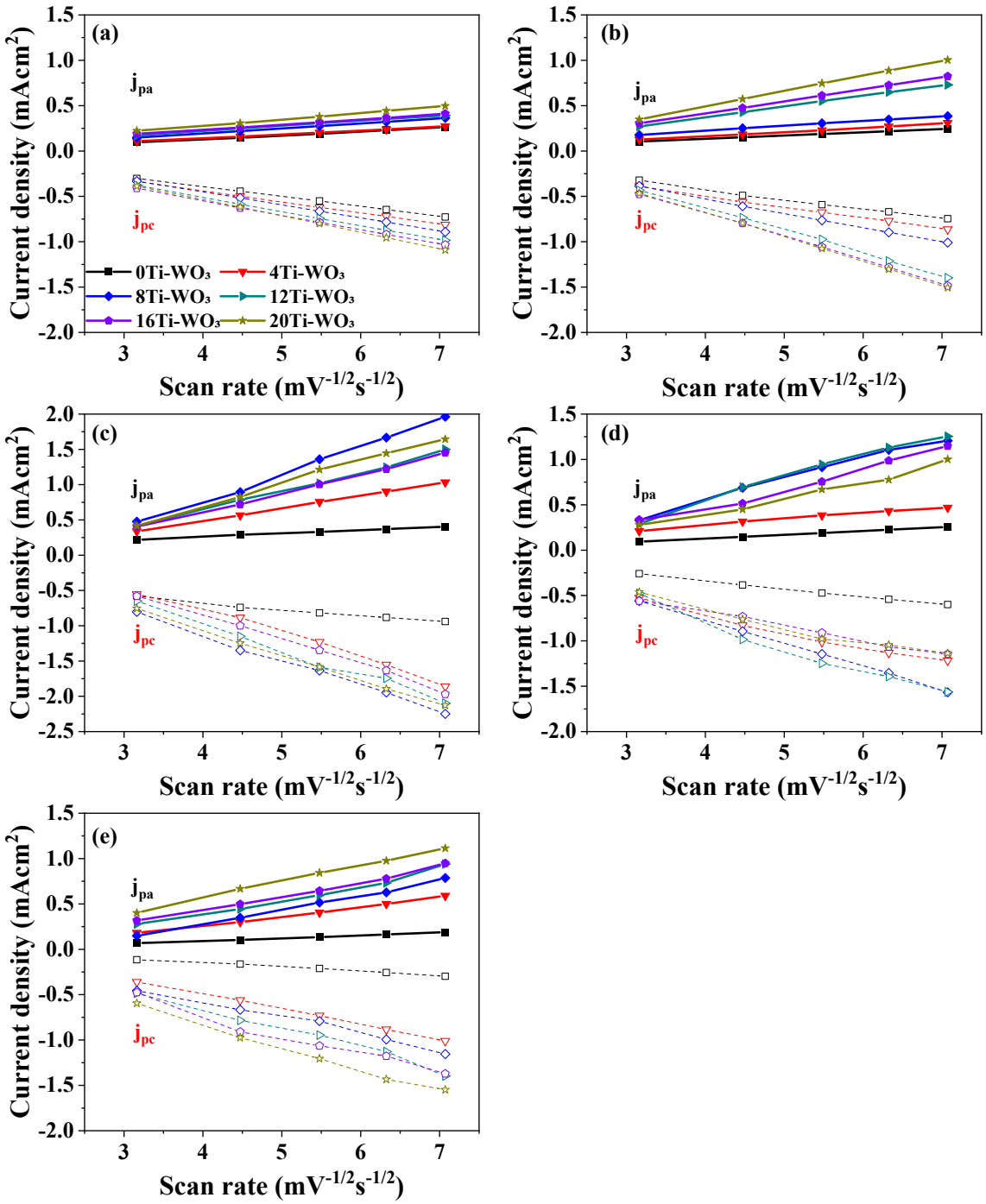

Figure S5. Calculations of diffusion coefficients of various WO_3 films annealed at (a) 200, (b) 250, (c) 300, (d) 350, and (e) 400 °C, respectively.

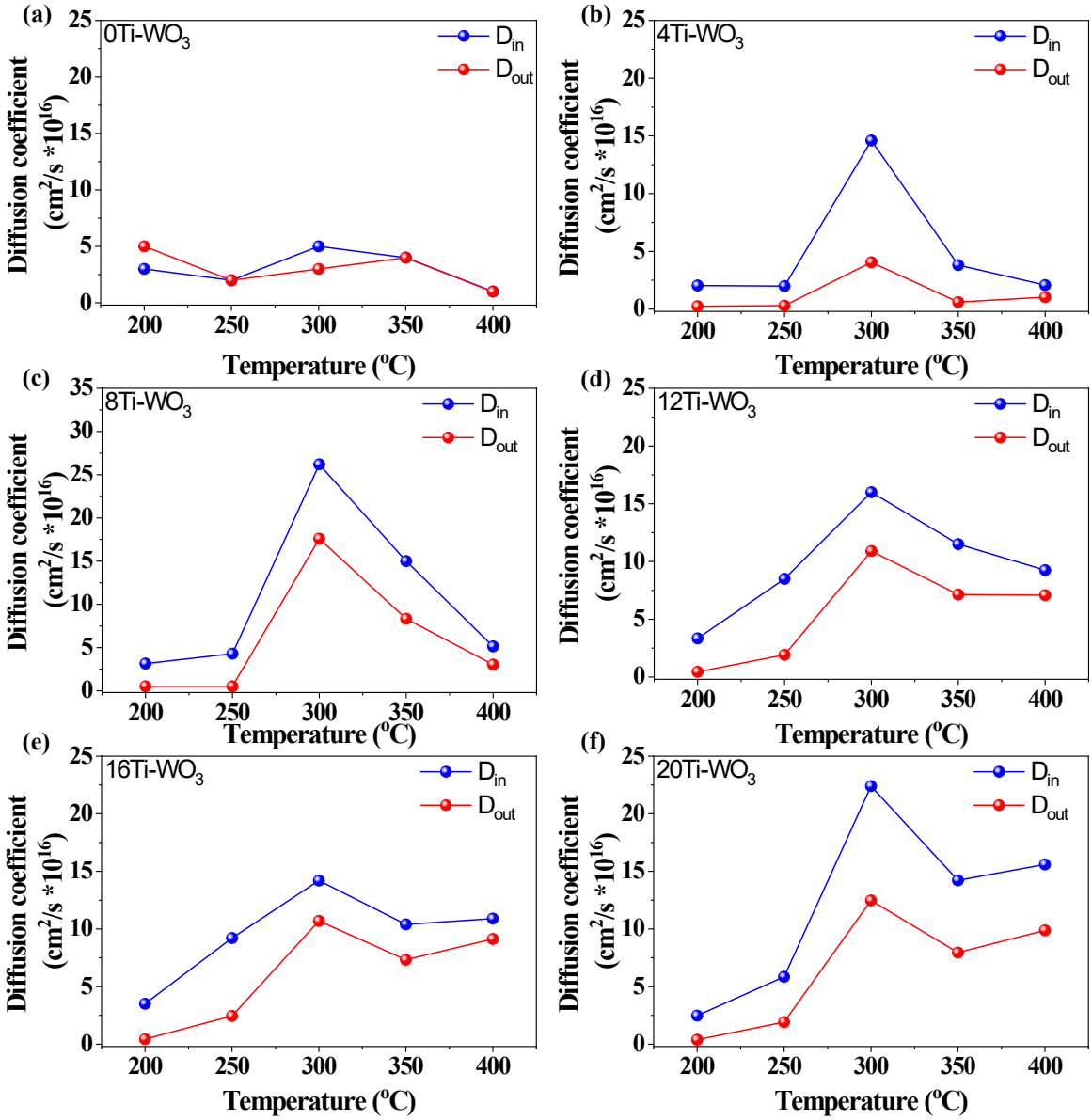

Figure S6. Calculated diffusion coefficients of (a) 0Ti-WO_3, (b) 4Ti-WO_3, (c) 8Ti-WO_3, (d) 12Ti-WO_3, (e) 16Ti-WO_3, and (f) 20Ti-WO_3 at various annealing temperatures.

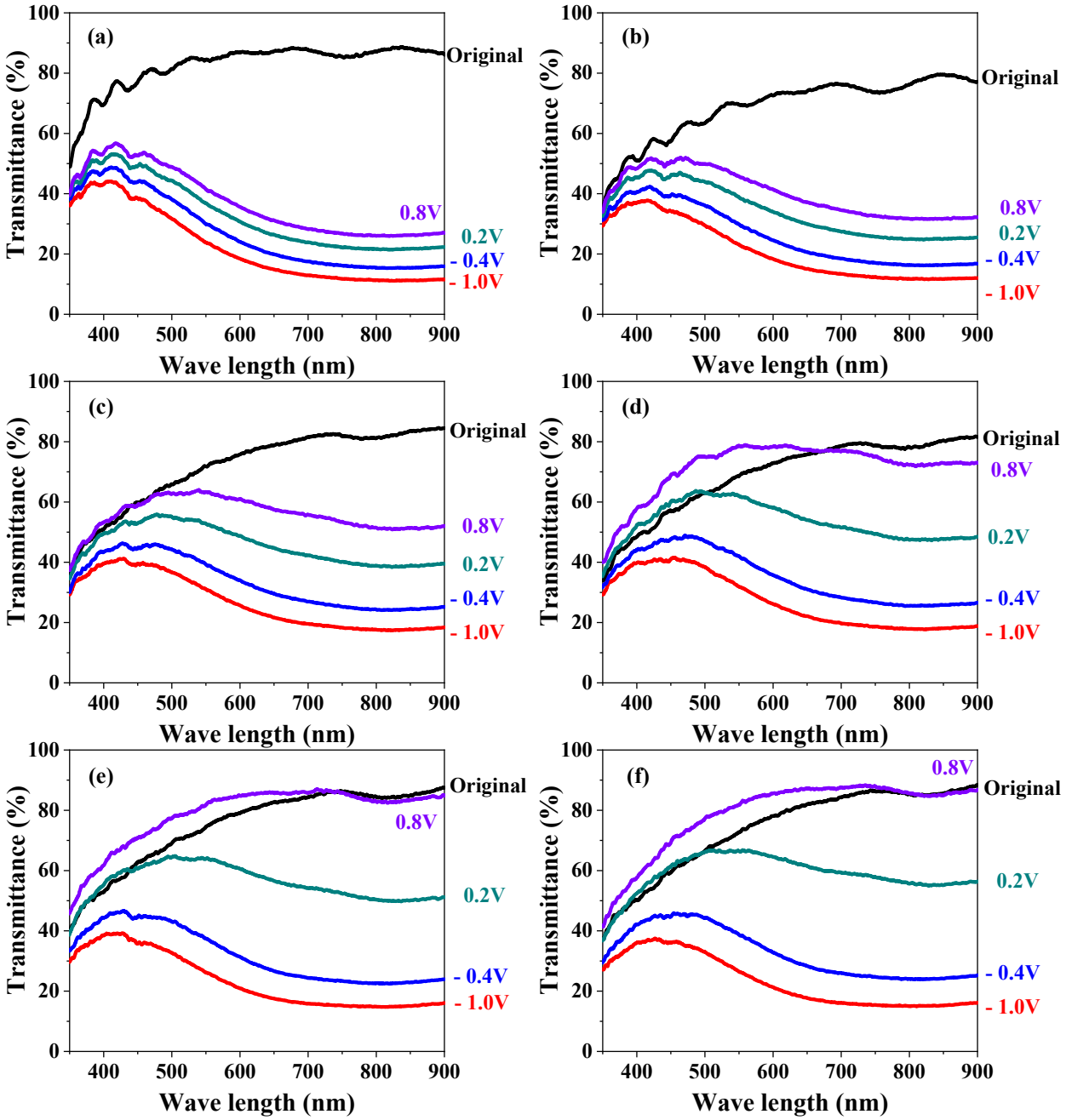

Figure S7. In-situ UV-Visible transmittance variations for (a) 0Ti-WO_3-200, (b) 4Ti-WO_3-200, (c) 8Ti-WO_3-200, (d) 12Ti-WO_3-200, (e) 16Ti-WO_3-200, and (f) 20Ti-WO_3-200, respectively.

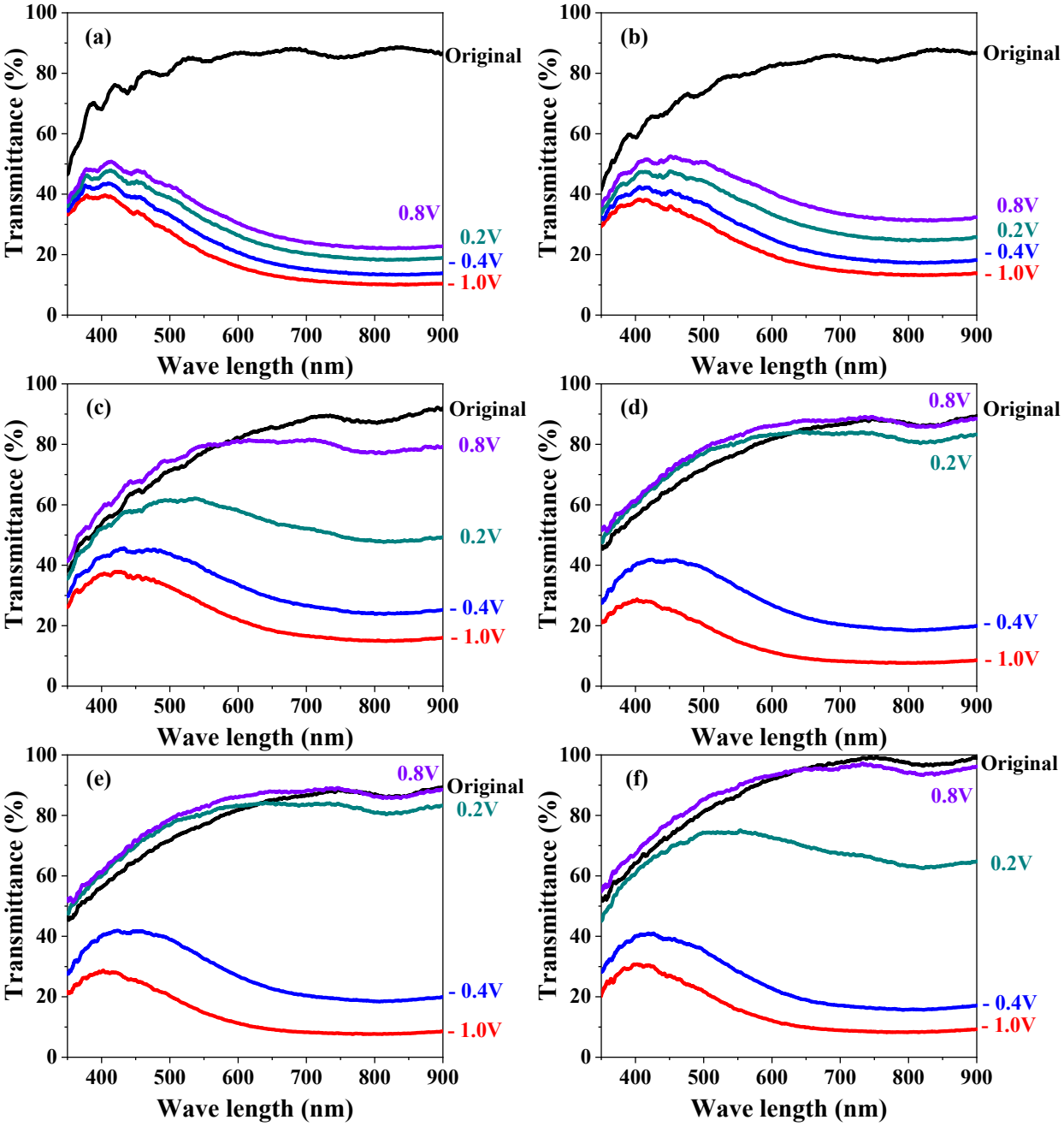

Figure S8. In-situ UV-Visible transmittance variations for (a) 0Ti-WO_3-250, (b) 4Ti-WO_3-250, (c) 8Ti-WO_3-250, (d) 12Ti-WO_3-250, (e) 16Ti-WO_3-250, and (f) 20Ti-WO_3-250, respectively.

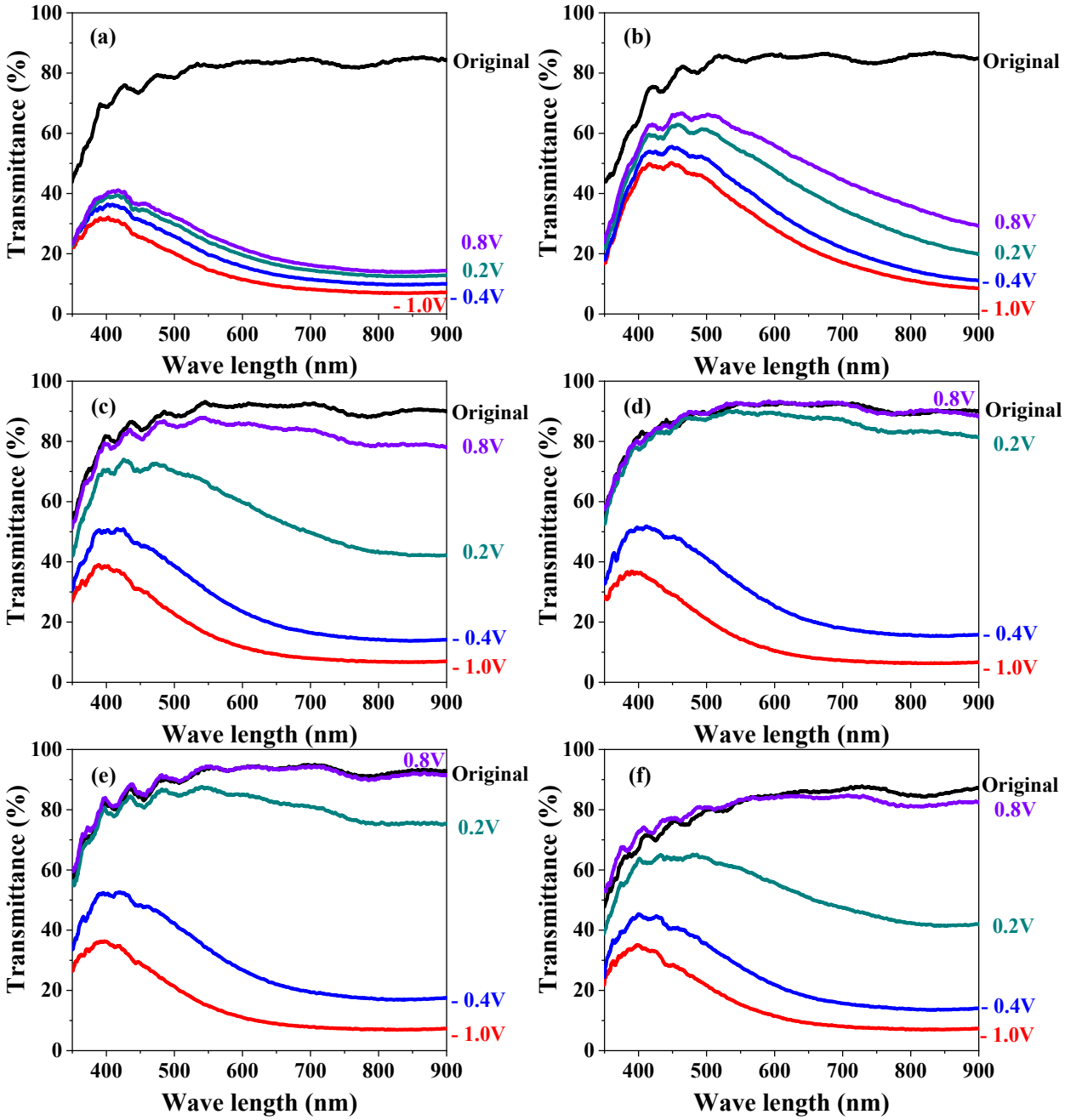

Figure S9. In-situ UV-Visible transmittance variations for (a) 0Ti-WO_3-350, (b) 4Ti-WO_3-350, (c) 8Ti-WO_3-350, (d) 12Ti-WO_3-350, (e) 16Ti-WO_3-350, and (f) 20Ti-WO_3-350, respectively.

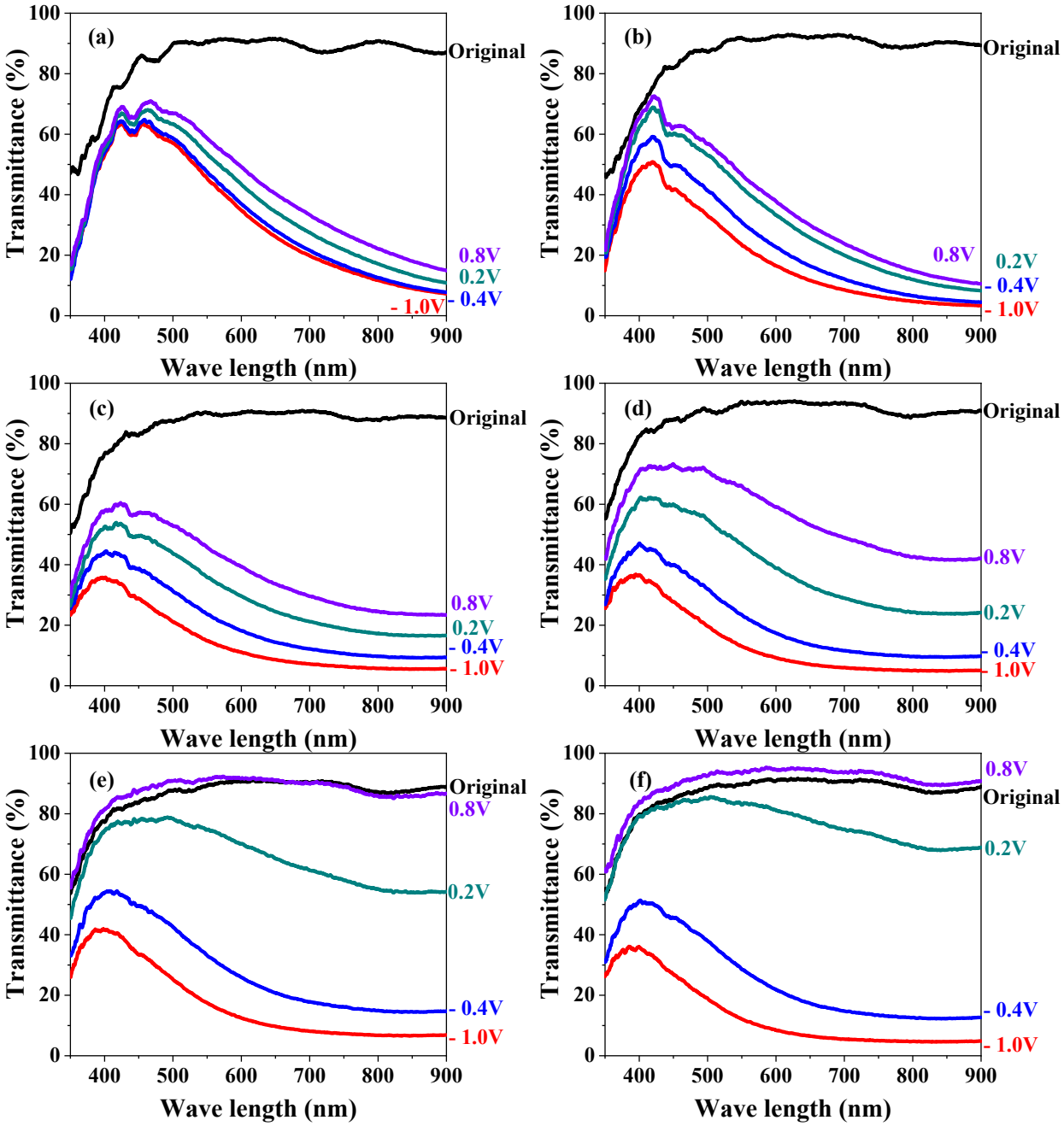

Figure S10. In-situ UV-Visible transmittance variations for (a) 0Ti-WO_3-400, (b) 4Ti-WO_3-400, (c) 8Ti-WO_3-400, (d) 12Ti-WO_3-400, (e) 16Ti-WO_3-400, and (f) 20Ti-WO_3-400, respectively.

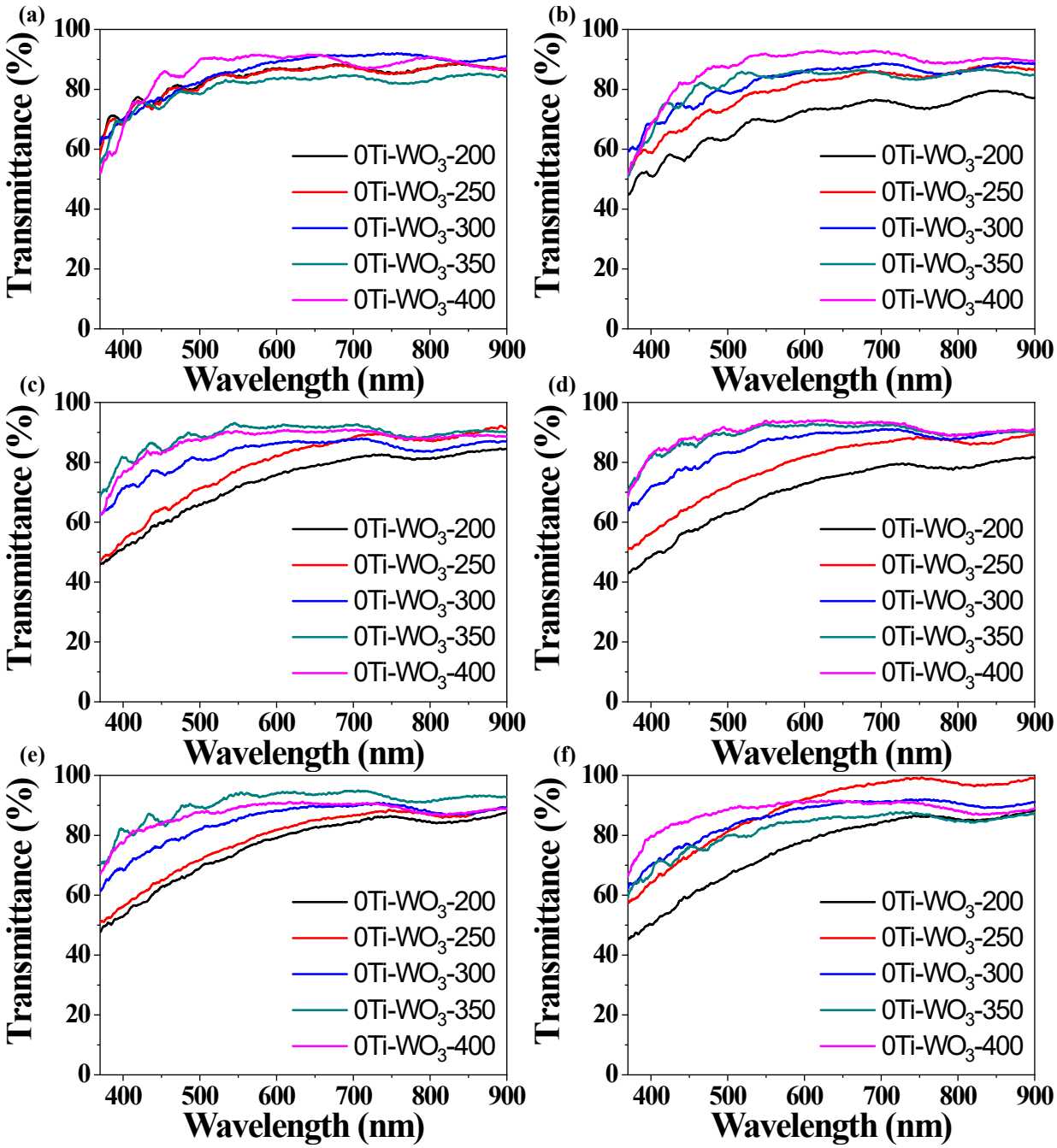

Figure S11. UV-Visible transmittance spectra of (a) 0Ti-WO_3, (b) 4Ti-WO_3, (c) 8Ti-WO_3, (d) 12Ti-WO_3, (e) 16Ti-WO_3, and (f) 20Ti-WO_3 at the pristine states under different annealing temperatures.

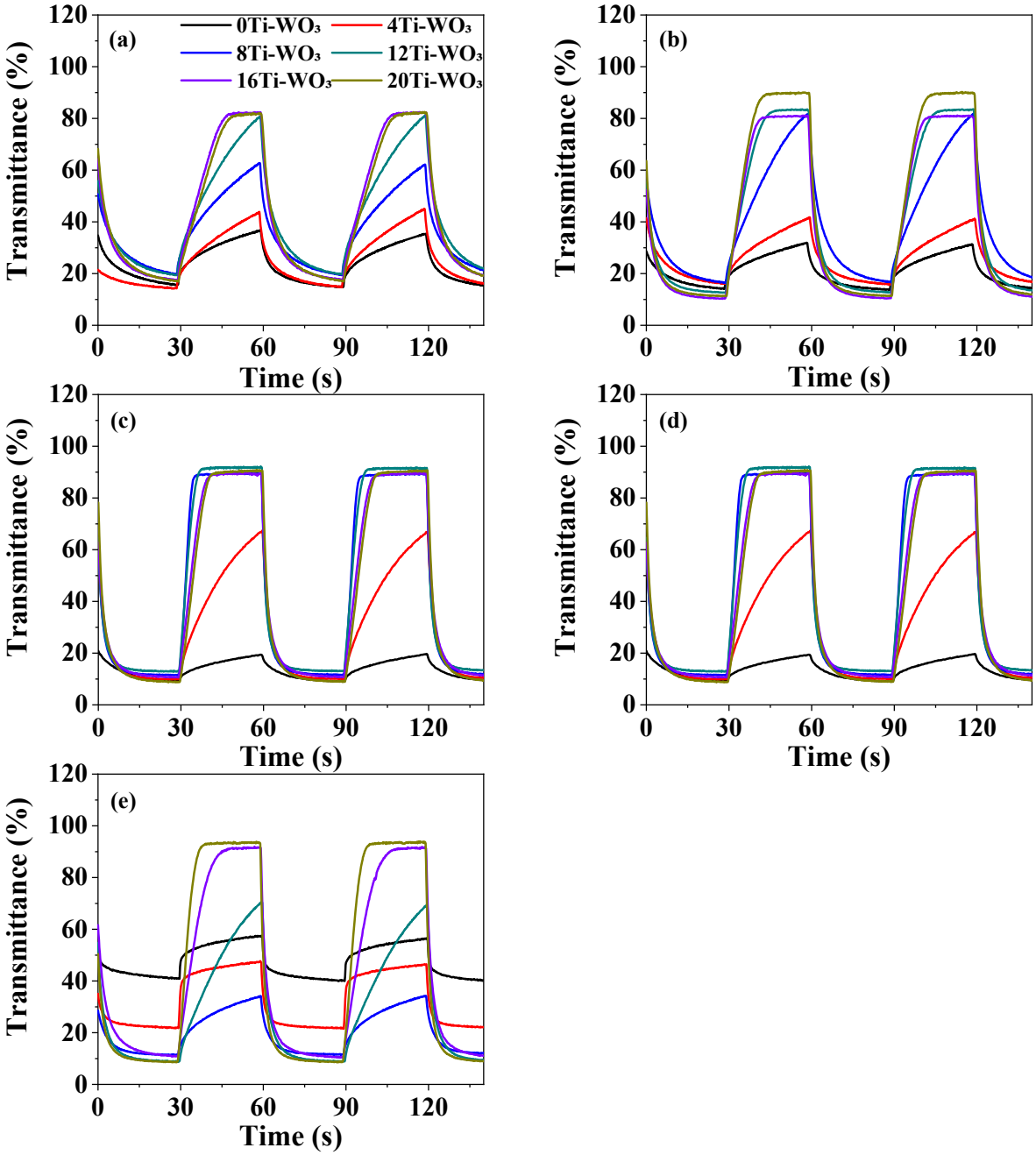

Figure S12. *In situ* optical response of the WO_3 films for 60 s per step measured at 550 nm annealed at (a) 200, (b) 250, (c) 300, (d) 350, and (e) 400 °C.

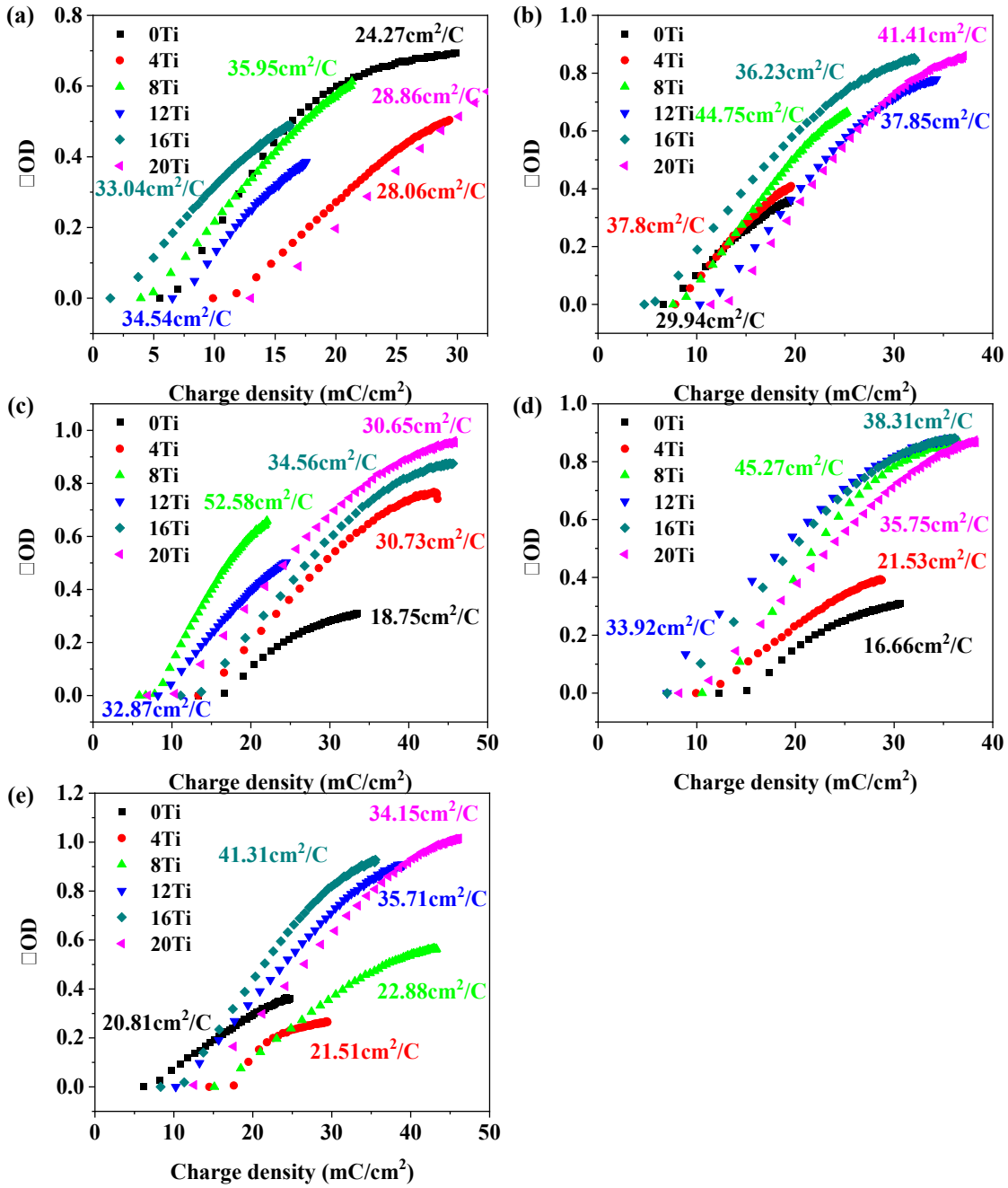

Figure S13. Optical density variation with respect to the charge density of WO_3 films annealed at (a) 200, (b) 250, (c) 300, (d) 350, and (e) 400 °C.

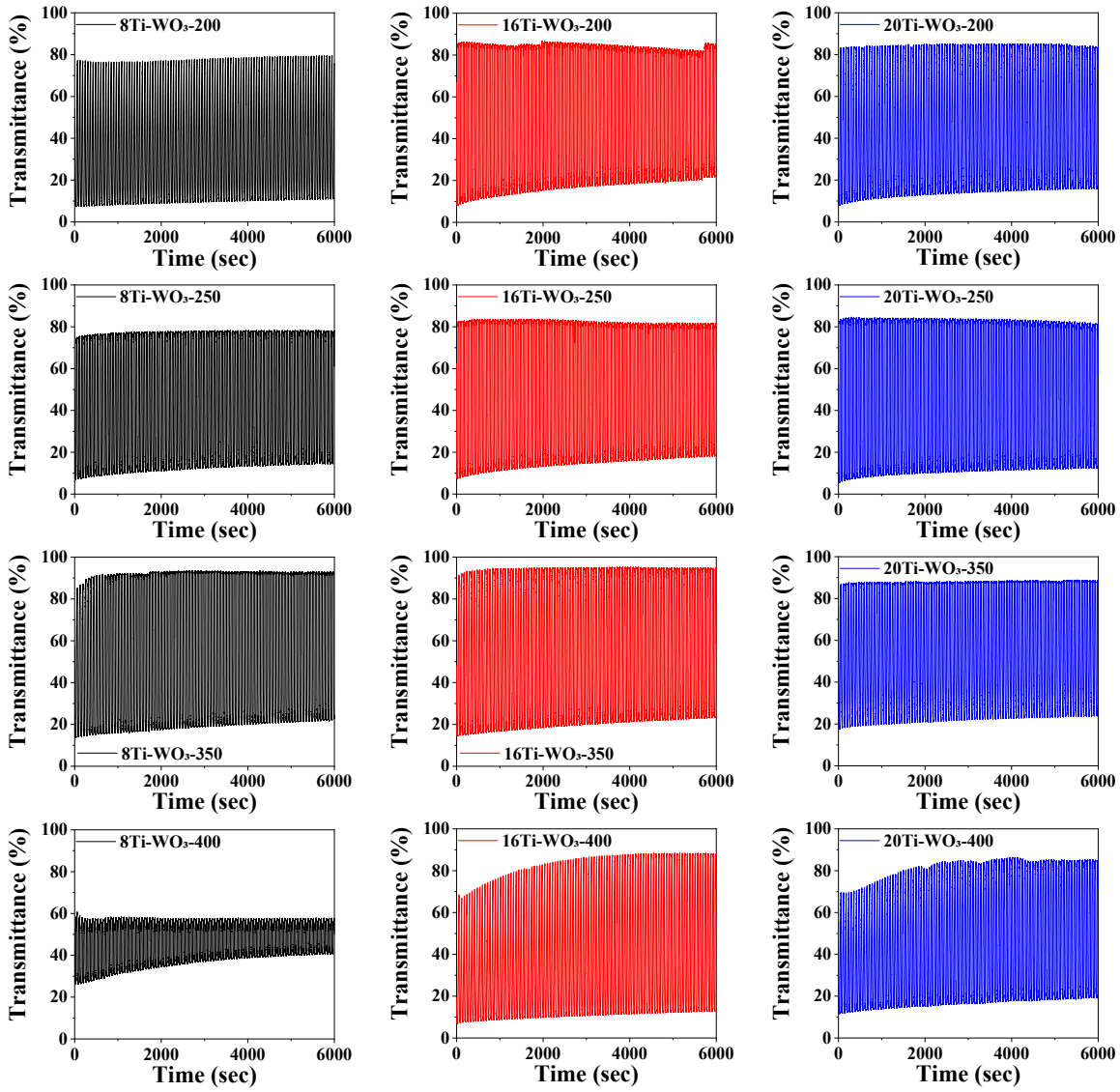

Figure S14. In-situ transmittance variation at λ=550 nm during cyclic tests for 8Ti-, 16Ti- and 20Ti-WO_3-films from left to right annealed at 200 (1st row), 250 (2nd row), 350 (3rd row) and 400 °C (4th row).